Progress In Electromagnetics Research B, Vol. 29, 139–155, 2011

ANALYSIS AND DESIGN OF CRUCIFORM WAVEGUIDE JUNCTION WITH A CONDUCTING DIAPHRAGM AND A DIELECTRIC LAYER IN THE MAIN ARM

F. G. Bogdanov and G. S. Kevanishvili

Telecommunications Department
Georgian Technical University, 77 Kostava Str., Tbilisi 0175, Georgia

G. V. Kekelia

D. Guramishvili International University Iberia
47 Khazbegi Ave., Tbilisi 0177, Georgia

S. L. Prosvirnin

Institute of Radio Astronomy
National Academy of Sciences of Ukraine
4 Krasnoznamennaya Str., Kharkiv 61002, Ukraine

Abstract—This paper proposes a rigorous theory of the H-plane four-port (cruciform) waveguide junction with a conducting diaphragm and a dielectric layer in the main (input) waveguide arm. This theory is based on the mode matching method in conjunction with Fourier transform technique and including the edge conditions in vicinity of the diaphragm edges. The numerical analysis of the cruciform waveguide junction is done, and optimal parameters of inclusions are predicted based on the minima of voltage standing wave ratio (VSWR) in the main arm.

1. INTRODUCTION

Multiport (three and higher order) waveguide junctions are widely used in microwave devices, such as directional couplers, filters, multiplexers, phase shifters, power dividers, etc. [1–6]. However, effectiveness of these devices is highly dependent on matching quality of waveguide arms, especially of the input arm with the energy supplied. Therefore,

Received 16 February 2011, Accepted 23 March 2011, Scheduled 28 March 2011
Corresponding author: Faik G. Bogdanov (faik.bogdanov@emcos.com).

different type artificial inclusions, such as cylindrical rods, metallic diaphragms, etc., are included in the junctions as adjusting elements to improve their matching properties [7, 8].

Recently, a lot of work has been published to analyse and design the three- and higher order multiport port waveguide junctions with different types of artificial inclusions [9–18]. Besides, various optimization techniques have been proposed to optimize the geometric and material parameters of these junctions [19–23]. However, though the three-port waveguide junctions have been faithfully studied in rigorous formulation, four-port and higher order junctions have been mainly considered in approximate way and, therefore, need the more careful consideration.

This paper develops a rigorous electromagnetic theory of the H-plane four-port (cruciform) waveguide junction with a conducting diaphragm and a dielectric layer in the main arm. The numerical analysis of scattering characteristics of such the junctions is done, optimal parameters of the diaphragm are predicted, and a near field structure of the total field in optimised cruciform waveguide junction is analysed.

2. METHOD

2.1. Boundary Problem Formulation

The geometry of the problem presented in Fig. 1 consists of 4-port H-plane waveguide junction with a symmetric diaphragm and a dielectric layer placed in the main arm. The main arm 1 and the bottom arm 6 of the junction have the widths a, whereas the branched (side) arms 4 and 5 have the widths b. The diaphragm consists of the two strips of the width Δ separated by the aperture of the width d. The distances from the strips to the upper and bottom waveguide junctures are, respectively, ℓ and L. The strips are assumed to be infinitely thin and perfectly conducting, whereas the dielectric layer filling an intermediate area 2 has permittivity ε. The origin of the Cartesian coordinate system is taken at the centre of the aperture.

Let the waveguide junction be excited by the fundamental waveguide wave (H_{10}) incident from the main arm 1. This wave is fully defined by the y component of the electric field given by

$$E_y^{inc} = \cos(\sigma_1 x) e^{-ih_1 z} \quad (z \le 0, |x| \le a/2) \tag{1}$$

where $h_1 = \sqrt{k_0^2 - \sigma_1^2}$, $\mathrm{Im} h_1 < 0$, $k_0 = 2\pi/\lambda$, $\sigma_1 = \pi/a$. Hereinafter, the time dependence is assumed to be $\exp(i\omega t)$ and is omitted. We seek for the electromagnetic field arisen in different areas of the structure

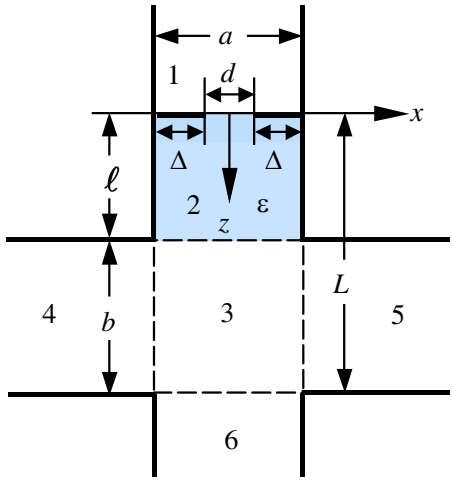

Figure 1. Cruciform waveguide junction with a diaphragm and dielectric layer in the input waveguide.

due to the diffraction of incident wave by diaphragm and waveguide junctures.

The total fields in areas 1, 2 and 6 are represented as Fourier series, and those in areas 3, 4, and 5 are represented as Fourier integrals in terms of modal spectra of reflected, transmitted, and interfering waves as:

$$E_{y1} = E_y^{inc} + \sum_{m=1}^{\infty} A_m \cos(\sigma_m x) e^{ih_m z} \quad (z \le 0,\ |x| \le a/2) \tag{2a}$$

$$E_{y2} = \sum_{m=1}^{\infty} [B_m e^{ih'_m(z-\ell)} + C_m e^{-ih'_m(z+\ell)}] \cos(\sigma_m x) \quad (0 \le z \le \ell,\ |x| \le a/2) \tag{2b}$$

$$E_{y3} = \int_{-\infty}^{\infty} dt \left\{ D(t) \mathrm{sh}\,[\alpha(t)(L-z)] + \tilde{D}(t) \mathrm{ch}\,[\alpha(t)(L-x)] \right\} e^{itx} \quad (\ell \le z \le L, -\infty < x < \infty) \tag{2c}$$

$$E_{y6} = \sum_{m=1}^{\infty} N_m \cos(\sigma_m x) e^{-ih_m(z-\ell)} \quad (z \ge L,\ |x| \le a/2) \tag{2d}$$

where $h_m = \sqrt{k_0^2 - \sigma_m^2}$, $h'_m = \sqrt{k^2 - \sigma_m^2}$, $\sigma_m = (2m-1)\pi/a$, $k = k_0\sqrt{\varepsilon_r}$, $\varepsilon_r = \varepsilon/\varepsilon_0$, $\alpha(t) = \sqrt{t^2 - k_0^2}$, and $\mathrm{Im}h_m < 0$, $\mathrm{Im}h'_m < 0$. In Eqs. (2a)–(2d), $\{A_m\}$ are the unknown Fourier amplitudes of modal

spectra of waves reflected from the diaphragm, $\{B_m\}$ and $\{C_m\}$ are those of waves interfering between the diaphragm and upper juncture, $D(t)$ and $\tilde{D}(t)$ are the amplitudes of continues Fourier spectra of waves interfering in the resonance area 3 and transmitted to the side arms 4 and 5, and $\{N_m\}$ are Fourier amplitudes of waves transmitted to the bottom arm 6.

The unknown coefficients $\{A_m\}$, $\{B_m\}$, $\{C_m\}$, $D(t)$, $\tilde{D}(t)$ and $\{N_m\}$ are to be determined from the zero boundary conditions on the surfaces of the conducting diaphragm ($z = 0, d/2 \le |x| \le a/2$) and side waveguide walls ($z = \ell, z = L, |x| \ge a/2$), and the continuity conditions on the interfaces between the areas 1 and 2, 2 and 3, and 3 and 6:

$$E_{y1} = E_{y2} \quad (z = 0,\ |x| \le a/2) \tag{3a}$$

$$E_{y2} = 0 \quad (z = 0,\ d/2 \le |x| \le a/2) \tag{3b}$$

$$\frac{\partial E_{y1}}{\partial z} = \frac{\partial E_{y2}}{\partial z} \quad (z = 0,\ |x| \le d/2) \tag{3c}$$

$$E_{y3} = \begin{cases} E_{y2} & (z = \ell,\ |x| \le a/2) \\ 0 & (z = \ell,\ |x| \ge a/2) \end{cases} \tag{3d}$$

$$\frac{\partial E_{y3}}{\partial z} = \frac{\partial E_{y2}}{\partial z} \quad (z = \ell,\ |x| \le a/2) \tag{3e}$$

$$E_{y3} = \begin{cases} E_{y6} & (z = L,\ |x| \le a/2) \\ 0 & (z = L,\ |x| \ge a/2) \end{cases} \tag{3f}$$

$$\frac{\partial E_{y3}}{\partial z} = \frac{\partial E_{y6}}{\partial z} \quad (z = L,\ |x| \le a/2) \tag{3g}$$

Besides, expansions (2a) and (2b) should satisfy the edge condition on the diaphragm plane ($z = 0$) as $|x| \to d/2$

$$\lim_{x \to \pm d/2} E_y(x)_{|z=0} \cong \text{const} \cdot \sqrt{1 - (2x/d)^2} = 0 \tag{4}$$

2.2. System of Functional Equations

Applying the boundary conditions (3a)–(3h) to (2a)–(2d) reduces the formulated problem to the following system of functional equations

$$\cos(\sigma_1 x) + \sum_{m=1}^{\infty} A_m \cos(\sigma_m x) = \sum_{m=1}^{\infty} (B_m + C_m)\, e^{-ih'_m \ell} \cos(\sigma_m x) \quad (|x| \le a/2) \tag{5a}$$

$$\sum_{m=1}^{\infty}(B_m+C_m)\,e^{-ih'_m\ell}\cos(\sigma_m x)=0 \quad (d/2\le|x|\le a/2) \tag{5b}$$

$$\begin{aligned}&\sum_{m=1}^{\infty}h'_m\,(B_m-C_m)\,e^{-ih'_m\ell}\cos(\sigma_m x)\\ =\;& -h_1\cos(\sigma_1 x)+\sum_{m=1}^{\infty}A_m h_m\cos(\sigma_m x) \quad (|x|\le d/2)\end{aligned} \tag{5c}$$

$$\begin{aligned}&\int\limits_{-\infty}^{\infty}dt\left\{D(t)\mathrm{sh}\,[\alpha(t)b]+\tilde{D}(t)\mathrm{ch}\,[\alpha(t)b]\right\}e^{itx}\\ =\;&\begin{cases}\sum\limits_{m=1}^{\infty}\left(B_m+C_m e^{-2ih'_m\ell}\right)\cos(\sigma_m x) & (|x|\le a/2)\\ 0, & (|x|\ge a/2)\end{cases}\end{aligned} \tag{5d}$$

$$\begin{aligned}&\int\limits_{-\infty}^{\infty}dt\alpha(t)\left\{D(t)\mathrm{ch}\,[\alpha(t)b]+\tilde{D}(t)\mathrm{sh}\,[\alpha(t)b]\right\}e^{itx}\\ =\;&-\sum_{m=1}^{\infty}ih'_m\left(B_m-C_m e^{-2ih'_m\ell}\right)\cos(\sigma_m x) \quad (|x|\le a/2)\end{aligned} \tag{5e}$$

$$\int\limits_{-\infty}^{\infty}\tilde{D}(t)e^{itx}dt=\begin{cases}N_m\cos(\sigma_m x) & (|x|\le a/2)\\ 0 & (|x|\ge a/2)\end{cases} \tag{5f}$$

$$\int\limits_{-\infty}^{\infty}D(t)\alpha(t)e^{itx}dt=\sum_{m=1}^{\infty}ih_m N_m\cos\sigma_m x \quad (|x|\le a/2) \tag{5g}$$

Besides, applying the edge condition (4) to (2b) allows the following expansion for the aperture field

$$\sum_{m=1}^{\infty}(B_m+C_m)\,e^{-ih'_m\ell}\cos(\sigma_m x)=\sum_{s=1}^{\infty}X_s U_{2s-1}[(2x/d] \quad (|x|\le d/2) \tag{5h}$$

where $U_{2s-1}(x)$ is the $(2s-1)$-th Chebyshev function of the second kind, and X_s are the unknown expansion coefficients. Thus, utilization of (5h) guarantees the solution to satisfy the edge condition (4).

2.3. Reduced System of Functional Equations

Let transform the system of functional Eqs. (5a)–(5h) to the reduced system being more convenient for further analysis. First, we use the

orthogonality of the transverse eigen-functions $\{\cos(\sigma_m x)\}_{m=1}^{\infty}$ on the segment $-a/2 \le x \le a/2$ to reduce (5a) to the following relation

$$(B_m + C_m)e^{-ih'_m\ell} = \delta_{m1} + A_m \tag{6}$$

where δ_{mn} denotes the Kronecker's delta.

Equation (6) is substituted into (5c) to obtain

$$\begin{aligned} &\sum_{m=1}^{\infty} [(h'_m + h_m)C_m - (h'_m - h_m)B_m]e^{-ih'_m\ell}\cos(\sigma_m x) \\ &= 2h_1\cos(\sigma_1 x) \quad (-d/2 \le x \le d/2) \end{aligned} \tag{7}$$

Further, we multiply Eqs. (5d) and (5f) by $e^{-it'x}$ and integrate over the interval $-\infty < t' < \infty$ to obtain the following relations between the coefficients of the continuous and discrete Fourier spectra

$$D(t)\mathrm{sh}[\alpha(t)b] + \tilde{D}(t)\mathrm{ch}[\alpha(t)b] = \frac{1}{2\pi}\sum_{m=1}^{\infty}\left(B_m + C_m e^{-2ih'_m\ell}\right)\Phi_m(t) \tag{8}$$

$$\tilde{D}(t) = \frac{1}{2\pi}\sum_{m=1}^{\infty} N_m \Phi_m(t) \tag{9}$$

where

$$\Phi_m(t) = (-1)^{m-1}\sigma_m \frac{e^{ita/2} + e^{-ita/2}}{\sigma_m^2 - t^2} \tag{10}$$

Next, we eliminate $\tilde{D}(t)$ from Eqs. (8) and (9) to yield

$$D(t) = \frac{1}{2\pi\mathrm{sh}[\alpha(t)b]}\sum_{m=1}^{\infty}\left[\left(B_m + C_m e^{-2ih'_m\ell}\right) - N_m\mathrm{ch}[\alpha(t)b]\right]\Phi_m(t) \tag{11}$$

Substituting Eqs. (9) and (11) into Eqs. (5e) and (5g) leads to the following functional equations:

$$\begin{aligned} &\sum_{m=1}^{\infty} ih'_m\left(B_m - C_m e^{-2ih'_m\ell}\right)\cos(\sigma_m x) \\ &= -\sum_{m=1}^{\infty}\left[\left(B_m + C_m e^{-2ih'_m\ell}\right)F_m(x) - N_m\tilde{F}_m(x)\right] \quad (|x| \le a/2) \end{aligned} \tag{12}$$

$$\begin{aligned} &\sum_{m=1}^{\infty} ih_m N_m \cos(\sigma_m x) \\ &= \sum_{m=1}^{\infty}\left[\left(B_m + C_m e^{-2ih'_m\ell}\right)\tilde{F}_m(x) - N_m F_m(x)\right] \quad (|x| \le a/2) \end{aligned} \tag{13}$$

where

$$F_m(x) = \frac{1}{2\pi}\int\limits_{-\infty}^{\infty}\frac{\alpha(t)\Phi_m(t)\mathrm{ch}\,[\alpha(t)b]}{\mathrm{sh}\,[\alpha(t)b]}e^{itx}dt \tag{14}$$

$$\tilde{F}_m(x) = \frac{1}{2\pi}\int\limits_{-\infty}^{\infty}\frac{\alpha(t)\Phi_m(t)}{\mathrm{sh}\,[\alpha(t)b]}e^{itx}dt \tag{15}$$

The integration in Eqs. (14) and (15) can be easily performed using the residual calculus to obtain

$$\begin{aligned}
F_m(x) &= (-1)^{m-1}\sigma_m\left\{(-1)^{m-1}\sqrt{\sigma_m^2-k_0^2}\frac{\mathrm{cth}(\sqrt{\sigma_m^2-k_0^2}b)}{\sigma_m}\cos(\sigma_m x)\right.\\
&\quad\left.+i\sum_{n=1}^{\infty}(t_n^2-k_0^2)\frac{e^{it_n(a/2+x)}+e^{it_n(a/2-x)}}{bt_n(\sigma_m^2-t_n^2)}\right\}\\
\tilde{F}_m(x) &= (-1)^{m-1}\sigma_m\left\{(-1)^{m-1}\frac{\sqrt{\sigma_m^2-k_0^2}}{\sigma_m\mathrm{sh}(\sqrt{\sigma_m^2-k_0^2}b)}\cos(\sigma_m x)\right.\\
&\quad\left.+i\sum_{n=1}^{\infty}(-1)^n(t_n^2-k_0^2)\frac{e^{it_n(a/2+x)}+e^{it_n(a/2-x)}}{bt_n(\sigma_m^2-t_n^2)}\right\}
\end{aligned}$$

where $t_n = -\sqrt{k_0^2-(\pi n/b)^2}$.

Finally, multiplying Eq. (5h) by the eigen-functions $\{\cos(\sigma_n x)\}_{n=1}^{\infty}$ and integrating over the segment $-a/2 \le x \le a/2$ leads to the following relations

$$(B_m + C_m)\,e^{-ih'_m\ell} = \frac{2}{2m-1}\sum_{s=1}^{\infty}X_s J_{2s-1}[(2m-1)\alpha] \tag{16}$$

where $\alpha = \pi d/(2a)$, and $J_{2s-1}(x)$ is the $(2s-1)$-th order Bessel function.

It can be shown, that Eq. (16) automatically satisfies Eq. (5b) that excludes it from further consideration. Thus, the initial system of functional Eqs. (5a)–(5h) is reduced to the equivalent system (7), (12) and (13) in terms of unknown coefficients B_m, C_m and N_m, with substitution of (16) to satisfy the edge condition (4).

2.4. System of Algebraic Equations

Let now reduce the obtained functional system to the algebraic equations convenient for the numerical analysis. First, we change the

variables in Eq. (7) as $\sigma_m x = (2m-1)\alpha\xi$, $\xi = 2x/d$ to use the following series expansion of trigonometric functions in domain $\xi \in [-1, 1]$

$$\begin{aligned}&\cos[(2m-1)\alpha\xi]\\ &= 2\sum_{n=1}^{\infty}(-1)^{n-1}(2n-1)\frac{J_{2n-1}\left[(2m-1)\alpha\right]U_{2n-1}(\xi)}{\alpha(2m-1)\sqrt{1-\xi^2}} \quad (-1 \le \xi \le 1)\end{aligned}$$

Using now the orthogonality of Chebyshev functions $\{U_{2n-1}(\alpha\xi)\}_{n=1}^{\infty}$ over the segment $-1 \le \xi \le 1$ yields the following set of algebraic equations

$$\sum_{m=1}^{\infty}(R'_{nm}C_m + R''_{nm}B_m) = a_n (n = 1, 2, 3\ldots) \tag{17}$$

where

$$\begin{aligned}a_n &= 2h_1(-1)^{n-1}(2n-1)\frac{J_{2n-1}(\alpha)}{\alpha} \qquad (17a)\\ R'_{nm} &= (h'_m + h_m)r_{nm}, R''_{nm} = -(h'_m - h_m)r_{nm}\\ r_{nm} &= e^{-ih'_m\ell}(-1)^{n-1}(2n-1)\frac{J_{2n-1}\left[(2m-1)\alpha\right]}{\alpha(2m-1)}\end{aligned}$$

Next, using the orthogonality of eigen-functions $\{\cos(\sigma_n x)\}_{n=1}^{\infty}$ on the segment $-a/2 \le x \le a/2$, we obtain from Eq. (12) the following set of algebraic equations, considered together with Eq. (17)

$$B_n - C_n e^{-2ih'_n\ell} = \sum_{m=1}^{\infty}\left[B_m + C_m e^{-2ih'_m\ell}\right]\tilde{Q}_{nm} + N_m\tilde{Q}'_{nm} \qquad (n = 1, 2, 3\ldots) \tag{18}$$

where

$$\tilde{Q}_{nm} = -2Q_{nm}/(ih'_n a), \tilde{Q}'_{nm} = 2Q'_{nm}/(ih'_n a) \tag{18a}$$

and

$$\begin{aligned}Q_{nm} &= \int_{-a/2}^{a/2} F_m(x)\cos(\sigma_m x)dx = (1)^{m-1}\sigma_m \times \left\{\frac{(1)^{m-1}\zeta_m}{\sigma_m \mathrm{th}(\zeta_m b)}\frac{a}{2}\delta_{nm}\right.\\ &\left. -2i(-1)^{n-1}\frac{\sigma_n}{b}\sum_{s=1}^{\infty}\frac{(h_s^{2''} - k_0^2)(1 + e^{-ih''_s a})}{h''_s(h_s^{2''} - \sigma_n^2)(h_s^{2''} - \sigma_m^2)}\right\} \qquad (18b)\\ Q'_{nm} &= \int_{-a/2}^{a/2} \tilde{F}_m(x)\cos(\sigma_m x)dx = (1)^{m-1}\sigma_m \times \left\{\frac{(1)^{m-1}\zeta_m}{\sigma_m \mathrm{sh}(\zeta_m b)}\frac{a}{2}\delta_{nm}\right.\\ &\left. -2i(-1)^{n-1}\frac{\sigma_n}{b}\sum_{s=1}^{\infty}\frac{(-1)^s(h2''_s - k_3^2)(1 + e^{-ih''_s a})}{h''_s(h_s^{2''} - \sigma_n^2)(h_s^{2''} - \sigma_m^2)}\right\} \qquad (18c)\end{aligned}$$

where $h''_n = \sqrt{k_0^2 - (n\pi/b)^2}$, $\zeta_m = \sqrt{\sigma_m^2 - k_0^2}$.

Applying now the same procedure to Eq. (13) yields the following set of algebraic equations, considered together with Eqs. (17) and (18)

$$-N_n = \sum_{m=1}^{\infty} \left(B_m + C_m e^{-2ih'_m \ell}\right) \hat{Q}'_{nm} + N_m \tilde{Q}''_{nm} \quad (n = 1, 2, 3 \ldots) \quad (19)$$

where

$$\tilde{Q}''_{nm} = -2Q_{nm}/(ih_n a), \quad \hat{Q}'_{nm} = 2Q'_{nm}/(ih_n a) \quad (19a)$$

Finally, using Eq. (16), we eliminate the unknowns C_m from the algebraic system (17) to (19) to meet the edge condition (4) and obtain the following triple set of linear algebraic equations

$$\begin{aligned} \sum_{s=1}^{\infty} (R_{ns} B_s + R^*_{ns} X_s) &= a_n \\ B_n b_n + \sum_{s=1}^{\infty} (P_{ns} B_s + P^*_{ns} X_s + \tilde{Q}'_{ns} N_s) &= 0 \quad (n = 1, 2, 3 \ldots) \\ -N_n + \sum_{s=1}^{\infty} (G_{ns} B_s + G^*_{ns} X_s + \tilde{Q}''_{ns} N_s) &= 0 \end{aligned} \quad (20)$$

where a_n is defined by Eq. (17a), and

$$R_{ns} = -2h'_s e^{-ih'_s \ell} (-1)^{n-1} (2n-1) \frac{J_{2n-1}\left[(2s-1)\alpha\right]}{\alpha(2s-1)} \quad (20a)$$

$$R^*_{ns} = \frac{2}{\alpha} (-1)^{n-1} (2n-1) \times \sum_{m=1}^{\infty} \frac{(h_m + h'_m) J_{2n-1}\left[(2m-1)\alpha\right] J_{2s-1}\left[(2m-1)\alpha\right]}{(2m-1)^2} \quad (20b)$$

$$P^*_{ns} = -\beta_n J_{2s-1}\left[(2n-1)\alpha\right] - \sum_{m=1}^{\infty} \beta_m \tilde{Q}_{nm} J_{2s-1}\left[(2m-1)\alpha\right] \quad (20c)$$

$$b_n = 1 + e^{-2ih'_n \ell}, \quad P_{ns} = -(1 - e^{-2ih'_s \ell}) \tilde{Q}_{ns}, \quad \beta_n = \frac{2e^{-ih'_n \ell}}{2n-1} \quad (20d)$$

$$G_{ns} = (1 - e^{-2ih'_s \ell}) \hat{Q}'_{ns}, \quad G^*_{ns} = \sum_{m=1}^{\infty} \beta_m \hat{Q}'_{nm} J_{2s-1}\left[(2m-1)\alpha\right] \quad (20e)$$

and $\tilde{Q}_{ns}$, $\tilde{Q}'_{ns}$, $\tilde{Q}''_{ns}$ and $\hat{Q}'_{ns}$ and are defined by Formulas (17a), (18a) to (18c) and (10a), respectively. The linear set (20) fully determines the solution to the boundary problem.

2.5. Field in the Side Branches and Power Balance Equation

After solution of the linear set (20), fields in the main arm (areas 1 and 2) and the bottom arm (area 6) of cruciform waveguide junction may be calculated using Eqs. (1), (2a), (2b), (2d), (6) and (16). However, calculation of fields in the resonance region 3 and the side branches 4 and 5 requires additional analytical treatment.

Substituting Eqs. (9) and (11) into Eq. (2c) yields

$$E_{y3} = \sum_{m=1}^{\infty} \left[\left(B_m + C_m e^{-2ih'_m \ell} \right) \Psi_m(x,z) + N_m \hat{\Psi}_m(x,z) \right] \qquad (\ell \le z \le L, -\infty < x < \infty) \tag{21}$$

where

$$\Psi_m(x,z) = \frac{1}{2\pi} \int_{-\infty}^{\infty} \frac{\Phi_m(t) \mathrm{sh}\left[\alpha(t)(L-z)\right]}{\mathrm{sh}[\alpha(t)b]} e^{itx} dt \tag{22}$$

$$\hat{\Psi}_m(x,z) = -\frac{1}{2\pi} \int_{-\infty}^{\infty} \frac{\Phi_m(t) \mathrm{sh}\left[\alpha(t)(\ell-z)\right]}{\mathrm{sh}[\alpha(t)b]} e^{itx} dt \tag{23}$$

and $\Phi_m(t)$ is defined by Eq. (10).

Equation (21) is applied to characterise the fields at all areas (3, 4 and 5) in side waveguide, but the results of integration in (22) and (23) depend on the chosen area (value of variable x). From the mathematical point of view, this is because of choosing different half planes for finding poles of integrand expressions. From the physical point of view, this is because of the change of physical meaning of the solution.

Thus, integration of (22) and (23) in area 3 yields

$$\Psi_m(x,z) = \cos(\sigma_m x) \frac{\mathrm{sh}\left[\zeta_m(L-z)\right]}{\mathrm{sh}(\zeta_m b)} - \frac{2i\sigma_m}{(-1)^{m-1}} \sum_{n=1}^{\infty} \frac{q_n e^{-ih''_n a/2} \cos(h''_n x)}{(-1)^n h''_n b (h_n^{2''} - \sigma_m^2)} \sin\left[q_n(L-z)\right], \quad |x| \le a/2 \tag{22a}$$

$$\hat{\Psi}_m(x,z) = -\cos(\sigma_m x) \frac{\mathrm{sh}\left[\zeta_m(\ell-z)\right]}{\mathrm{sh}(\zeta_m b)} + \frac{2i\sigma_m}{(-1)^{m-1}} \sum_{n=1}^{\infty} \frac{q_n e^{-ih''_n a/2} \cos(h''_n x)}{(-1)^n h''_n b (h_n^{2''} - \sigma_m^2)} \sin\left[q_n(\ell-z)\right], \quad |x| \le a/2 \tag{23a}$$

where $q_n = \pi n/b$. Eqs. (22a) and (23a) describe the standing waves in resonance area 3.

The integration of (22) and (23) in areas 4, 5 yields

$$\Psi_m(x,z) = -2i(-1)^{m-1}\sigma_m \times \sum_{n=1}^{\infty} \frac{q_n(-1)^n \cos(h_n''a/2)}{bh_n''(h_n^{2''}-\sigma_m^2)} \sin\left[q_n(L-z)\right] e^{\pm ih_n''x}, \quad |x| \geq a/2 \tag{22b}$$

$$\hat{\Psi}_m(x,z) = 2i(-1)^{m-1}\frac{\sigma_m}{h_n^{2''}-\sigma_m^2} \times \sum_{n=1}^{\infty} \frac{q_n \cos(h_n''a/2)}{bh_n''} \sin\left[q_n(L-z)\right] e^{\pm ih_n''x}, \quad |x| \geq a/2 \tag{23b}$$

where "+" sign in exponents stands for area 4 ($x < -a/2$), and "−" sign stands for area 5 ($x > a/2$). Eqs. (22b) and (23b) describe the outgoing waves in the side waveguide arms 4 and 5.

Substituting Eqs. (22b) and (23b) in Eq. (21) and changing the order of the summations allows rewriting it in more convenient form

$$E_{y4,5} = \sum_{n=1}^{\infty} T_n \sin\left[q_n(L-z)\right] e^{\pm ih_n''x} \quad (\ell \leq z \leq L,\ |x| \geq a/2) \tag{24}$$

where

$$T_n = -2(-1)^n i \frac{q_n \cos(h_n''a/2)}{bh_n''} \times \sum_{m=1}^{\infty} \left[B_m + C_m e^{-2ih_m'\ell} - N_m(-1)^n\right](-1)^{m-1}\frac{\sigma_m}{h_n^{2''}-\sigma_m^2}$$

are the amplitudes of modal spectra of waves transmitted into the side waveguide arms 4 and 5.

The field representations (1), (2a), (2e) and (21) define the power balance equation in cruciform waveguide junction written in normalized form as

$$\sum_{m=1}^{M}(\hat{P}_{1m}+\hat{P}_{6m}) + \sum_{n=1}^{N}(\hat{P}_{4m}+\hat{P}_{5m}) = 1 \tag{25}$$

where

$$\hat{P}_{1m} = \frac{h_m}{h_1}|A_m|^2$$

$$\hat{P}_{4n} = \hat{P}_{5n} = \frac{h_n''b}{h_1 a}|T_n|^2$$

and

$$\hat{P}_{6m} = \frac{h_m}{h_1}|N_m|^2$$

are the normalized reflected and transmitted powers in the main, side and bottom waveguide arms, respectively, and M and N denote the numbers of propagating modes in these arms. Eq. (25) may be used to validate the accuracy of the solution from the energetic point of view.

3. NUMERICAL RESULTS AND DISCUSSION

The obtained solution (20) has been numerically investigated for different truncation indexes N_{tr}, geometry parameters b/a, inclusion parameters ℓ/a, d/a, ε_r and frequency parameters $2a/\lambda$. It has been stated, that a stable solution with a graphical accuracy is obtained already for $N_{tr} = 5$ to 7. It has been also verified, that power balance Eq. (25) is satisfied with accuracy 10^{-10}, besides the points of generating of new waveguide modes. Finally, the near field structure has been investigated to confirm, that the obtained solution satisfies all the boundary conditions. Hence, this solution totally satisfies the formulated problem [24].

Further, the obtained solution was used to calculate the scattering characteristics and find the optimal parameters of the included diaphragm ensuring minimum reflection in the main arm of the cruciform waveguide junction at the desired frequency band. Let demonstrate them first for equal arm widths ($b/a = 1$) and missed dielectric filling ($\varepsilon_r = 1$).

Figures 2(a) and (b) present the maps of voltage standing wave ratio (VSWR) in the main arm of the cruciform waveguide junction versus the frequency parameter $2a/\lambda$ and geometric parameters of the diaphragm. The different colours in palette maps correspond to different values (levels) of VSWR, which are shown on the scroll bars on the right. Thus, the dark blue colour area in the maps corresponds to the minimum VSWR (minimum reflection) in the main arm given the values of optimal geometric parameters of the diaphragm. These optimal parameters of inclusions are dependent on the chosen frequency range (regime of propagation). So, chosen the frequency range $2a/\lambda = 1.75$ to 1.85, the optimal diaphragm parameters are found to be $\ell/a = 0.56$, $d/a = 0.67$.

Figure 3 shows the frequency behavior of the reflected and transmitted powers in cruciform waveguide junction for the diaphragm parameters $\ell/a = 0.56$, $d/a = 0.67$. These graphs illustrate a rather good power balance performance in waveguide junction and allow determining the frequency bands with admissible reflection. Thus,

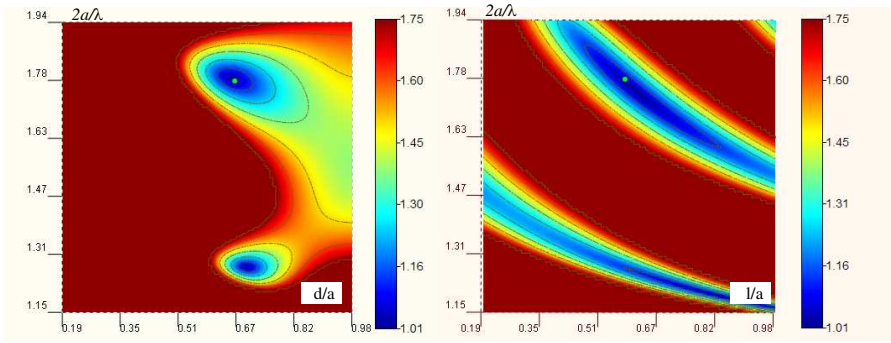

Figure 2. VSWR maps in cruciform waveguide junction with a conducting diaphragm for $b/a = 1$, $\varepsilon_r = 1$ and different diaphragm parameters: (a) $\ell/a = 0.56$, (b) $d/a = 0.67$.

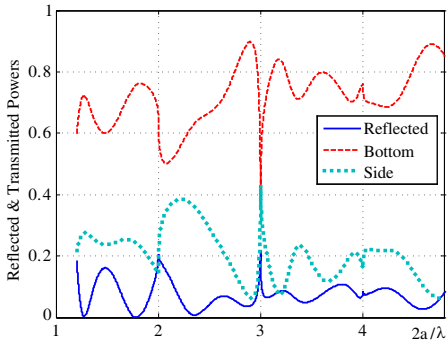

Figure 3. Energetic characteristics of cruciform waveguide junction with a conducting diaphragm versus the frequency parameter $2a/\lambda$ at diaphragm parameters $\ell/a = 0.56$, $d/a = 0.67$.

in one-mode regime of propagation minimum reflection is observed for $2a/\lambda = 1.28$ and 1.78.

Figure 4 demonstrates a near field structure in waveguide junction calculated at optimal diaphragm parameters $\ell/a = 0.56$, $d/a = 0.67$, $2a/\lambda = 1.78$. This figure illustrates the boundary conditions performance in waveguide junction, allows evaluating the peak values of the electric field nearby the resonance region, and demonstrates the formation of a regular field structure nearby the juncture regions.

Finally, Figs. 5(a) and (b) show the VSWR maps in the main arm of the cruciform waveguide junction with a conducting diaphragm and

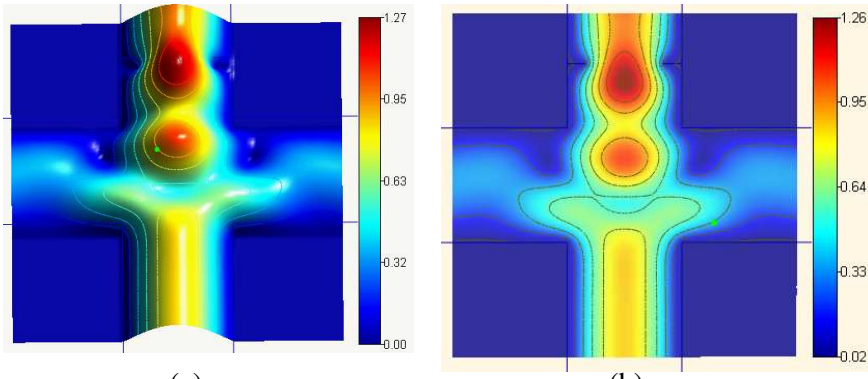

Figure 4. The electric field structure in the y-cut plane of waveguide junction with a conducting diaphragm for $b\alpha = 1$, $\varepsilon_r = 1$ and optimal diaphragm parameters $\ell/a = 0.56$, $d/a = 0.67$, $2a/\lambda = 1.78$: (a) 3D-view, (b) 2D-view.

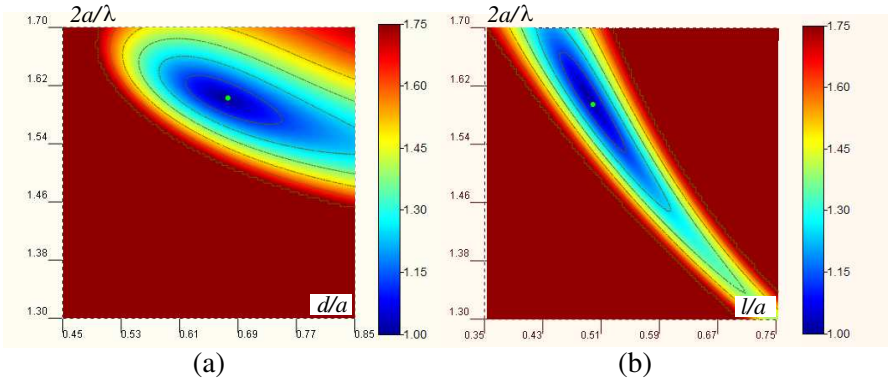

Figure 5. VSWR maps in cruciform waveguide junction with a conducting diaphragm for $b/a = 1$, $\varepsilon_r = 2.1$ and different diaphragm parameters: (a) $\ell/a = 0.49$, (b) $d/a = 0.67$.

dielectric layer ($\varepsilon_r = 2.1$). For the comparison, Fig. 5(b) is calculated for the same diaphragm gap ($d/a = 0.67$), as that in Fig. 2(b). It is seen, that the presence of dielectric results in the shift of the optimal distance ℓ/a and the decrease of the operation frequency corresponding to minimum reflection. Thus, the presence of the metallic and dielectric inclusions allows one to find the optimal regime of propagation in cruciform waveguide junction with minimum reflection in the main arm.

It should be noted that the described optimization strategy allows only optimization of the main (input) waveguide arm. It results in a number of the sets of optimized parameters. The further selection of the acceptable optimized set should be done depending on the specification of the designed device. The more severe specification requires the further modification of the structure by including additional adjusting elements to match each waveguide juncture and considering the multi-parameter optimization strategy.

4. CONCLUSIONS

In this work, a rigorous theory has been developed for H-plane four-port (cruciform) waveguide junction with a conducting diaphragm and a dielectric layer in the main arm. The scattering characteristics of such a junction have been analysed, and optimal parameters of inclusions have been predicted based on the palette maps for the voltage standing wave ratio (VSWR) versus the parameters of inclusions in the main arm of the junction.

ACKNOWLEDGMENT

This work was supported in part by the Science and Technology Center in Ukraine (STCU), under Grant Project N 4390.

REFERENCES

1. Arndt, F., I. Ahrens, U. Papziner, U. Wiechmann, and R. Willkeit, "Optimized E-plane T-junction series power dividers," *IEEE Trans. Microwave Theory Techn.*, Vol. 35, 1052–1059, 1987.
2. Alessandri, F., et al., "Admittance matrix formulation of waveguide discontinuity problems: Computer-aided design of branch guide directional couplers," *IEEE Trans. Microwave Theory and Techniques*, Vol. 36, No. 2, 394–403, Feb. 1988.
3. Itoh, T., Ed., *Numerical Techniques for Microwave and Millimeter Wave Passive Structures*, Wiley, New York, 1989.
4. Ruiz-Cruz, J. A., J. R. Montejo-Garai, J. M. Rebollar, and S. Sobrino, "Compact full Ku-band triplexer with improved E-plane power divider, *Progress In Electromagnetics Research*, Vol. 86, 39–51, 2008.
5. Lopez-Berrocal, B., J. De-Oliva-Rubio, E. Marquez-Segura, A. Moscoso-Martir, I. Molina-Fernandez, and P. Uhlig, "High performance 1.8–18 GHz 10-dB low temperature co-fired ceramic

directional coupler," *Progress In Electromagnetics Research*, Vol. 104, 99–112, 2010.

6. Shamsinejad, S., M. Soleimani, and N. Komjani, "Novel enhanced and miniaturized 90° coupler for 3G EH mixers," *Progress In Electromagnetics Research Letters*, Vol. 3, 43–50, 2008.
7. Schwinger, J. and D. S. Saxon, *Discontinuities in Waveguides*, Gordon & Breach, New York, 1968.
8. Guglielmi, M. and C. Newport, "Rigorous, multimode equivalent network representation of inductive discontinuities," *IEEE Trans. Microwave Theory and Tech.*, Vol. 38, No. 11, 1651–1659, Nov. 1990.
9. Wu, K.-L. and H. Wang, "Rigorous modal analysis of *H*-plane waveguide T-junction loaded with a partial-height post for wide-band applications," *IEEE Trans. Microwave Theory Tech.*, Vol. 49, 893–901, May 2001.
10. Kishihara, M., I. Ohta, and K. Yamane, "Cruciform directional couplers in *E*-plane rectangular waveguide," *IEICE Trans. Electron.*, Vol. E90-C, No. 9, 1743–1748, Sep. 2007.
11. Chen, H. and Y. X. Zhang, "A novel compact planar six-way power divider using folded and hybrid-expanded coupled lines," *Progress In Electromagnetics Research*, Vol. 76, 243–252, 2007.
12. Abdalla, M. A. and Z. Hu, "On the study of left-handed coplanar waveguide coupler on ferrite RN substrate," *Progress In Electromagnetics Research Letters*, Vol. 1, 69–75, 2008.
13. Abdalla, M. A. Y., K. Phang, and G. V. Eleftheriades, "A compact highly reconfigurable CMOS MMIC directional coupler," *IEEE Trans. Trans. Microwave Theory Techn.*, Vol. 56, No. 2, 305–319, Feb. 2008.
14. Al-Zayed, A. S. and S. F. Mahmoud, "Seven ports power divider with various power division ratios," *Progress In Electromagnetics Research*, Vol. 114, 383–393, 2011.
15. Bogdanov, F. G., G. S. Kevanishvili, G. V. Jandieri, G. V. Kekelia, and K. Yasumoto, "Simulation and analysis of multiport waveguide junctions with artificial discontinuities formed of the inductive strips and diaphragms," *PIERS Proceedings*, 125–128, Pisa, Italy, 2004.
16. Bogdanov, F., G. Kevanishvili, D. Kim, G. Jandieri, and K. Yasumoto, "Analysis and design of multiport waveguide junctions with artificial inclusions made of cylindrical rods," *Research Reports on Information Science and Electrical Engineering of Kyushu University*, Vol. 11, No. 1, 1–16, Fukuoka, Japan,

Mar. 2006.

17. Bogdanov, F. G., K. Yasumoto, G. S. Kevanishvili, G. V. Jandieri, and G. V. Kekelia, "Rigorous analysis of multiport waveguide junctions with diaphragms," *Conference Digest of IRMMW-THz 2006*, 538, 2006.
18. Bogdanov, F. G., G. S. Kevanishvili, G. V. Jandieri, G. V. Kekelia, and D. I. Kim, "Electromagnetic theory of four-port (cruciform) waveguide junction with a cylindrical rod," *Proceedings of International Symposium on Antennas and Propagation (ISAP-2005)*, 821–824, Seoul, Korea, Aug. 2005.
19. Lee, H.-B. and T. Itoh, "A systematic optimum design of waveguide-to-microstrip transition," *IEEE Trans. Trans. Microwave Theory Techn.*, Vol. 45, No. 5, 803–809, May 1997.
20. Hirayama, K., et al., "Application of topology optimization to H-plane waveguide component," *IEICE Trans. Electron.*, Vol. E90-C, No. 2, 1743–1748, 282–287, Feb. 2007.
21. Bogdanov, F. G., G. S. Kevanishvili, G. V. Jandieri, and D. I. Kim, "Simulation and optimization of waveguide junctions with artificial discontinuities including strips and dielectric layer," *Proceedings of IX International Seminar/Workshop on Direct and Inverse Problems of Electromagnetic and Acoustic Wave Theory (DIPED-2004)*, 47–50, Lviv-Tbilisi, 2004.
22. Bogdanov, F. G., G. S. Kevanishvili, G. V. Jandieri, and K. Yasumoto "Optimization strategy for multiport waveguide junctions with canonical types of artificial discontinuities," *Proceedings X International Symposium on Microwave and Optical Technology*, 625–627, Osaka, Japan, 2005.
23. Bogdanov, F. G., G. S. Kevanishvili, G. V. Jandieri, and K. Yasumoto, "Optimization strategy for multiport waveguide junctions with canonical types of artificial discontinuities," *International Journal of Microwave and Optical Technology*, Vol. 1, No. 2, 259–266, Aug. 2006.
24. Mittra, R. and W. W. Lee, *Analytical Techniques in the Theory of Guided Waves*, Macmillan, New York, 1971.